Active Acoustic Resonators with Reconfigurable Resonance Frequency, Absorption, and Bandwidth

Theodoros T. Koutserimpas,[1] Etienne Rivet,[2] Hervé Lissek,[3] and Romain Fleury[1,*]

[1] *Laboratory of Wave Engineering, École Polytechnique Fédérale de Lausanne (EPFL), 1015 Lausanne, Switzerland*

[2] *Logitech, EPFL Innovation Park, 1015 Lausanne, Switzerland*

[3] *Signal Processing Laboratory 2, École Polytechnique Fédérale de Lausanne (EPFL), 1015 Lausanne, Switzerland*

(Received 28 August 2019; revised manuscript received 10 October 2019; published 27 November 2019)

Acoustic resonators play a key role in the development of subwavelength-sized technologies capable of interacting with airborne audible sound, from its emission and absorption to its manipulation and processing. Specifically, artificial acoustic media made from an ensemble of subwavelength resonators, namely, acoustic metamaterials and metasurfaces, have enabled sound manipulation possibilities well beyond what is typically achievable using natural materials. Yet, the transition of such concepts from physics-driven explorations to practical applications has been drastically hindered by the major difficulty in controlling the resonance frequency, absorption level, and bandwidth of these resonators, making acoustic metamaterials often too narrowband, or sensitive to disorder and absorption losses. Here, we demonstrate the relevance of active electroacoustic resonators to address such limitations. We propose a feedback control scheme for loudspeakers (used as acoustic scatterers), which involves passband current control based on real-time sensing and processing of the pressure signal by field-programmable gate-array technologies. We demonstrate externally reconfigurable subwavelength acoustic resonators with independently tunable levels of absorption (including near-zero and near-one), bandwidth, and resonance frequency. We believe that this work demonstrates a viable route to overcome the current limitations of metamaterials and enable their practical applications.

DOI: 10.1103/PhysRevApplied.12.054064

I. INTRODUCTION

Acoustic devices, which manipulate and control sound signals, have been of great interest to the physics and engineering communities over the years. In particular, subwavelength arrangements of small acoustic resonators are at the basis of locally resonant metamaterials that have shown intriguing wave propagation properties [1–4], such as rainbow-trapping and broadband absorbers, tunable periodic waveguides, negative-refraction index, and imaging [5–10]. The extraordinary physical phenomena provided by acoustic metamaterials are generally not available with natural acoustic media and can provide a path for unconventional handling of waves, leading to revolutionized wave devices [11]. The evolution of localized acoustic metamaterials has bestowed uncommon sound-wave properties and applications. It opens up a platform for sound control, such as the manipulation of effective material properties [12], parity-time symmetric devices and sensors [13,14], frequency-selective acoustic metasurfaces and adaptive wavefield shaping [15,16], constant amplitude sound waves in disordered media [17], acoustic lenses with superresolution and imaging [18], asymmetric energy transport [19], analog computing [20], acoustic bianisotropy [21], and the realization of real-time and broadband acoustic cloaking and holography [22]. Although passive acoustic metamaterials are used to provide anomalous scattering properties and extreme values of constitutive parameters, they are unavoidably prone to losses and generally display narrowband functionalities, as direct consequences of the Kramers-Kronig relations, which must hold in any passive and causal material. In addition, acoustic metamaterials require fine tuning of the geometry and arrangement of an ensemble of resonators, thus making them generally sensitive to fabrication imperfection and resonance frequency disorder, which lead to imperfect isotropy and open up undesired band gaps. Here, we tackle these physical limitations by introducing active electroacoustic resonators. We provide and test a realistic platform for the realization of devices capable of controlling the scattering properties of subwavelength electroacoustic resonators, bridging the gap between theoretical research and physical implementation. This article has a broad range of interest as it allows the manipulation,

*romain.fleury@epfl.ch

at will, of the scattering properties of acoustic resonances, based on a combination of the transduction of electric energy to acoustic waves, wave interference, and the utilization of field-programmable gate-array (FPGA) technologies. Specifically, we demonstrate a class of acoustic resonant scatterers with externally tunable resonance bandwidth and frequency and externally controlled absorption level. We use the transduction property of electroacoustic resonators to implement an active feedback control based on time-domain processing of the sensed pressure signal, reinjecting a passband current signal properly related to the sensed acoustic pressure, thus creating an acoustic resonance with controllable properties. We experimentally demonstrate our scheme in one-dimensional scenarios involving a loudspeaker used as a resonant acoustic scatterer and embedded in a cylindrical pipe supporting a single propagating mode. Two configurations, which are useful to create synthetic acoustic materials or surfaces, are considered: (a) the loudspeaker is placed at the end of a tube, as shown in Fig. 1(a), with its back loaded by a closed box (only reflection and absorption are present); and (b) the loudspeaker is placed in the middle of the tube [Fig. 1(b), reflection, transmission, and absorption are present]. Our goal is to demonstrate that, in these two scenarios, it is possible to control the resonance of the acoustic admittance of the loudspeaker, with fully adjustable center frequency, bandwidth, and real value (inverse of acoustic resistance) at resonance [Fig. 1(c)], by using a carefully engineered feedback control strategy. The paper is organized as follows: in Sec. II, we briefly recall the linear model used to describe the principal physical system involved. This model sets the necessary basis to explain the proposed complex-envelope active-feedback control scheme, which is developed in Sec. III. In Sec. IV, we report results from experimental measurements to demonstrate that the method allows the resonance frequencies, resonance bandwidth, and real acoustic admittance of the loudspeakers to be controlled independently, for both the closed-box and in-tube configurations (as shown in Fig. 1). Finally, in Sec. V, we discuss our results and comment on the practical applications of our findings to current topics of interests in the field of synthetic acoustic matter.

II. LOUDSPEAKER MODEL AND CONTROL MECHANISM

The electrodynamic loudspeaker is an electroacoustic element, which is mechanically driven by a voice coil within a magnetic field. The acting forces are considerably small enough that we can adopt a linear model for the sound pressure at the front and back of the loudspeaker. It consists of three parts: acoustic, mechanical, and electrical parts. The frequency domain equation that describes the loudspeaker model is [23,24]

$$S_d \Delta p = Z_{\mathrm{MS}} u + Bli, \tag{1}$$

where S_d is the effective surface area of the loudspeaker (which generally differs from the physical cross-section area of the tube, S_t); $\Delta p = p^+ - p^-$ is the pressure difference at the front and back of the loudspeaker; u is the velocity; Bl is the force factor (which depends on the magnetic field and length of the coil); i is the current flowing through the voice coil; and $Z_{\mathrm{MS}} = R_{\mathrm{MS}} + j\omega M_{\mathrm{MS}} + \frac{1}{j\omega C_{\mathrm{MS}}}$ is the mechanical impedance, which describes a spring-mass-damper system with mechanical resistance R_{MS}, mass M_{MS}, and compliance C_{MS}. All parameters of the electrodynamic loudspeaker can be found by calibration. For the case of the closed-box loudspeaker [Fig. 1(a)], the closed-volume loading at the back allows us to recast the problem and eliminate the variable p^-, by relating it to the

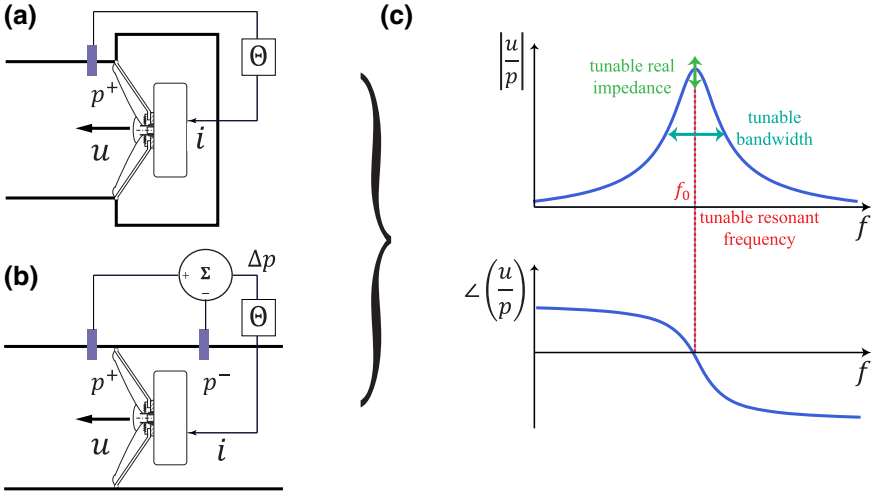

FIG. 1. (a) A tube terminated by a closed-box loudspeaker, (b) a loudspeaker in the middle of the tube, and (c) a schematic presentation of the effects of the control of the acoustic impedance.

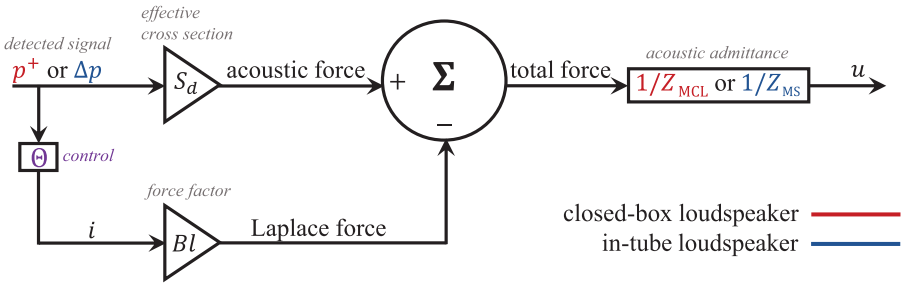

FIG. 2. Block diagram of the electrodynamic loudspeaker model with control parameter Θ. Red, closed-box loudspeaker; blue, in-tube loudspeaker. This diagram exhibits the control mechanism examined. As the pressure signal is detected, its value is multiplied by control parameter Θ and gives us the right value of the current. The current is injected back in real time to the loudspeaker and alters the particle velocity, resulting in the manipulation of the lumped element impedance.

membrane velocity, u, using acoustic compliance $C_{ab} = v_b/(\rho_0 c^2)$, where v_b is the volume of the enclosure and $p^- = (S_d u)/(j\omega C_{ab})$. In this case, Eq. (1) becomes

$$S_d p^+ = \underbrace{\left(Z_{\mathrm{MS}} + \frac{S_d^2}{j\omega C_{ab}}\right)}_{Z_{\mathrm{MCL}}} u + Bli. \tag{2}$$

The closed-box [Eq. (1)] and in-tube [Eq. (2)] models are both of the form

$$S_d p = Z_{\mathrm{M}} u + Bli, \tag{3}$$

where p is Δp for in-tube systems and p^+ for closed-box systems, and the mechanical impedance Z_{M} is analogously Z_{MS} for in-tube and Z_{MCL} for closed-box systems. Our control strategy relies on a feedback system that senses p and

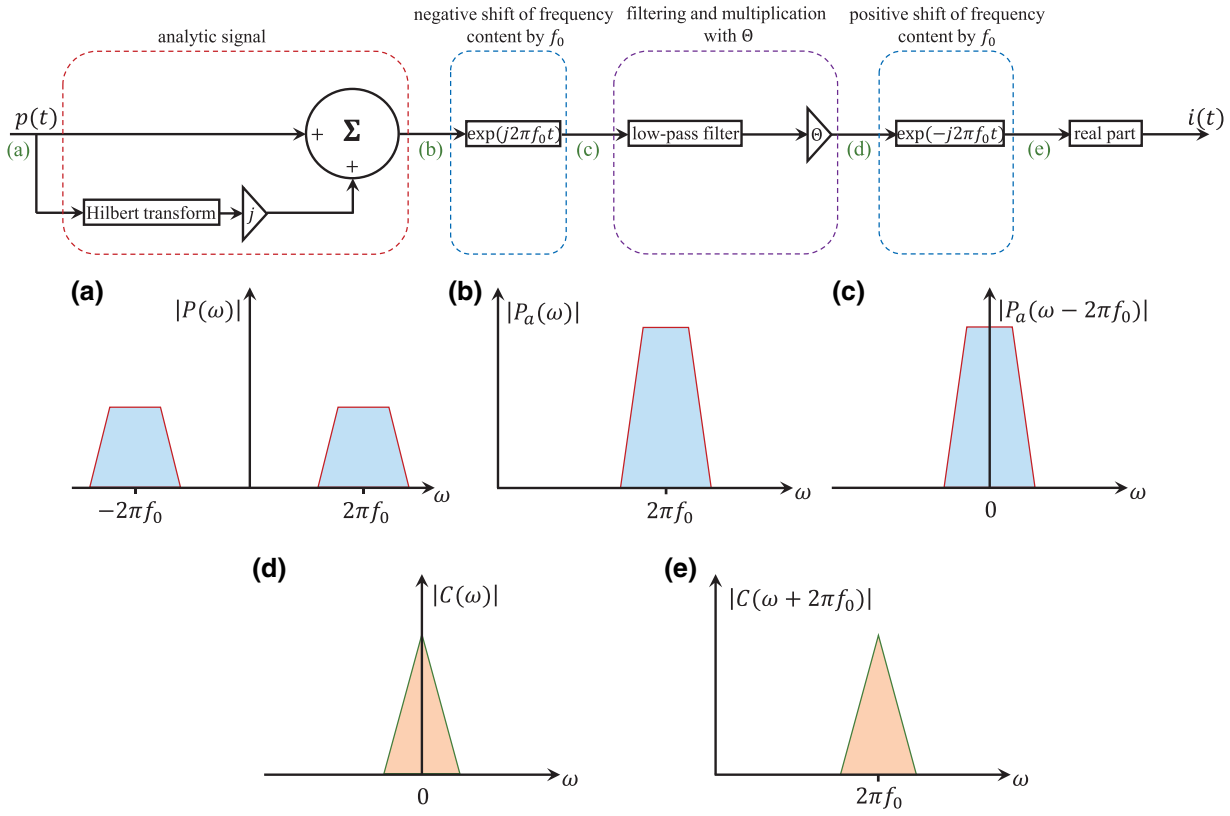

FIG. 3. Block diagram of acoustic pressure signal processed by the complex envelope technique and the corresponding frequency content of the signals under modulation: (a) frequency content of pressure signal $p(t)$, (b) frequency content of analytic signal $p_a(t)$, (c) negative frequency shift by the central frequency f_0, (d) application of low-pass filter and multiplication by the control parameter Θ, and (e) positive frequency shift by f_0.

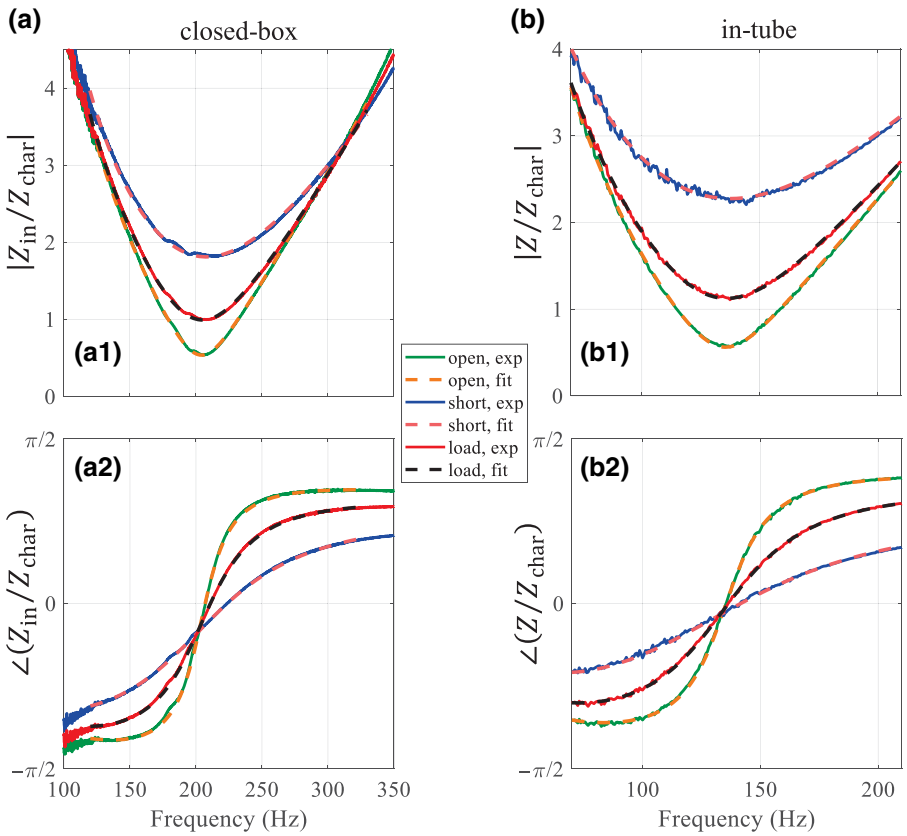

FIG. 4. Graphical plots for (a) closed-box and (b) in-tube systems under examination. (a1),(b1) show the amplitude and (a2),(b2) the phase of the normalized impedances for three independent cases: open circuit, short circuit, and load. Solid lines, measured data; dashed lines, results of fitting model.

applies a control current i, with $i = \Theta p$, where Θ represents the transfer function of the controller. The quantity that we aim to control is the acoustic impedance of the loudspeaker normalized by the cross section (as explained in the Appendix):

$$Z_s = \frac{p}{uS_d} = \frac{Z_M}{S_d^2} + \frac{Bli}{uS_d^2}. \tag{4}$$

Assuming that we require the impedance of the loudspeaker to take a desired value Z_c at frequency f_0, we obtain from Eqs. (3) and (4) a formula that gives the value that the control parameter Θ should take at that particular frequency:

$$\Theta = \frac{S_d}{Bl}\left(1 - \frac{Z_s}{Z_c}\right). \tag{5}$$

Similarly, we can control the acoustic impedance over a broad frequency interval by implementing the transfer function $\Theta(\omega)$, which is possible, as long as this transfer function is causal [23]. Figure 2 displays a block diagram for the loudspeaker under control.

However, here, our purpose is to induce a controllable resonance, similar to that in Fig. 1. This means that we only need to control the current over a narrow frequency range around a target resonance frequency value, f_0. Such narrowband control allows us to assign a desired real value to the impedance at resonance and tune the bandwidth. Sec. III describes how such a narrowband control strategy can be implemented in real time.

III. COMPLEX ENVELOPE TECHNIQUE

As described in Sec. II, we can always tailor the frequency distribution of $\Theta(\omega)$ and achieve acoustic wave properties on demand, as long as causality permits it and the linear model is valid [17,23,24]. More specifically, we aim to induce a resonance at a specific central frequency, f_0, targeting real values of impedance, $\{\mathrm{Im}[Z_c(2\pi f_0)] = 0\}$, and injecting current, $i = p\Theta$, over a narrow bandwidth around f_0. Since our objective is to control a small fraction of the frequency spectrum in real time, we design a reconfigurable band-pass system. To achieve that, we have to jump back and forth into time- and frequency-domain signal-processing techniques to implement a complex envelope control technique, as represented in Fig. 3. First, we detect, in real time, the pressure signal $p(t)$ and construct the component $p_h(t)$ of its time-domain complex analytic signal, which is defined as $p_a(t) = p(t) + jp_h(t)$, where $p_h(t)$ is the Hilbert transform of $p(t)$. One of the important properties of the analytic signal is that its frequency content satisfies $\mathcal{F}\{p_a(t)\} = P_a(\omega) = 2\mathcal{F}\{p(t)\}H(\omega)$, where $H(\omega)$ is the Heaviside distribution [as shown in Fig. 3(b)]. Working with the analytic signal is merely a trick to avoid dealing with the complex

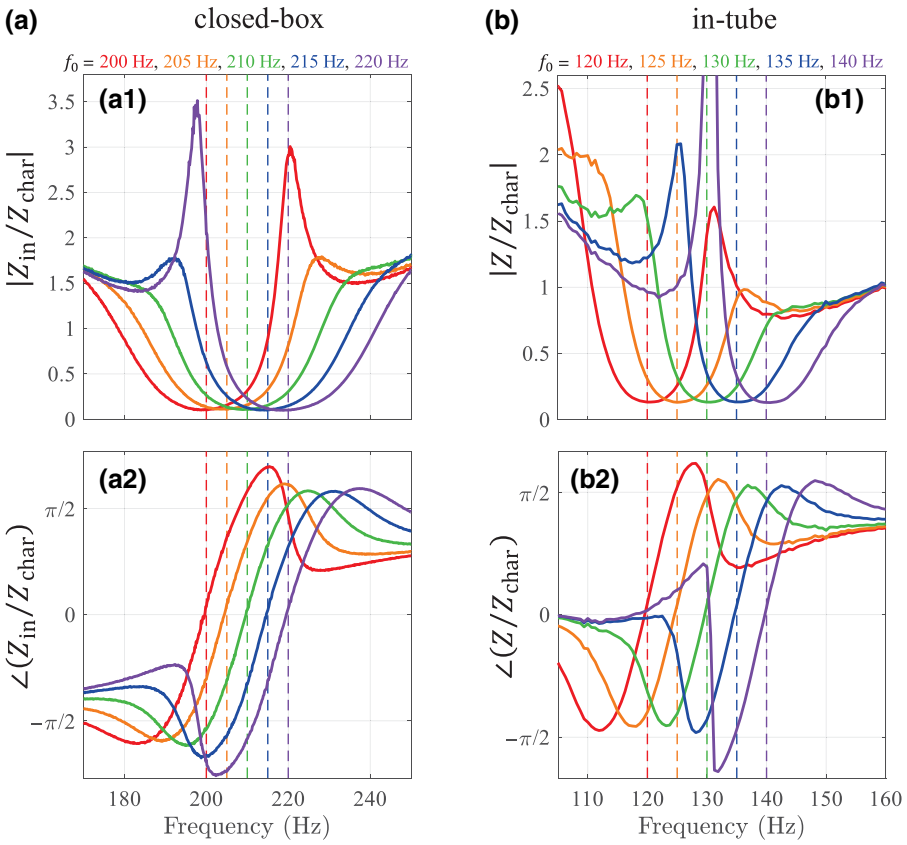

FIG. 5. Measured closed-box (a) and in-tube (b) electrodynamic loudspeaker impedance. For the closed-box system, the central frequency f_0 is shifted from 200 to 220 Hz with $B = 10$ Hz and $Z_{in}/Z_{char} = 0.1$. For the in-tube system, the central frequency f_0 is shifted from 120 to 140 Hz with $B = 5$ Hz and $Z/Z_{char} = 0.15$. (a1),(b1) are graphical presentations of the amplitude and (a2),(b2) of the phase of the acoustic impedance.

conjugate content of $\mathcal{F}\{p(t)\}$ at negative frequencies [25]. Knowing the target central frequency f_0 of the controlled resonator, we then compute the complex envelope signal: $p'(t) = p_a(t)e^{j2\pi f_0 t}$. It is clear that $P'(\omega) = P_a(\omega - 2\pi f_0)$, which results in a negative shift of the frequency distribution of the analytic signal by f_0, as shown in Fig. 3(c). The signal $p'(t)$ is therefore centered at zero frequency and can be filtered by a low-pass filter $L(2\pi B)$. The choice of the low-pass filter and its bandwidth B will determine the ultimate dispersion and bandwidth of the controlled resonance. We then multiply the signal by the constant value $\Theta(2\pi f_0)$ [as defined in Eq. (5)], which corresponds to the demanded real impedance at the central frequency f_0. The resulting signal is (in the frequency domain) $C(\omega) = \Theta(2\pi f_0)L(2\pi B)P_a(\omega - 2\pi f_0)$ [as shown in Fig. 3(d)]. After this analysis, it is straightforward to compute the required driving current: by positively shifting back the signal by f_0 units [as shown in Fig. 3(e)], the driving current is $i(t) = \mathrm{Re}[\mathcal{F}^{-1}\{C(\omega)\}e^{-j2\pi f_0 t}]$. Notably, the resulting control parameter, due to the complex envelope technique, is $\Theta(\omega - 2\pi f_0) = \Theta(2\pi f_0)L(2\pi B)$, where $\Theta(2\pi f_0)$ is a constant value and controls the real acoustic impedance value at the central frequency, while the choice of filter defines the scattering properties for the rest of the frequencies, in particular, the resonant bandwidth.

IV. EXPERIMENTAL RESULTS

In this section, we present experimental results for two representative cases: (a) a closed-box resonator and (b) an in-tube resonator. A low-pass Bessel filter of the second order is used to filter the shifted analytic pressure signal because it offers a reasonably flat and smooth area between the edges (other type of filters can be also used). The experimental setup consists of a power amplifier driving a source loudspeaker connected to a rigid tube, the controlled loudspeaker (either closed-box or in-tube), and a set of 130F20 microphones that are used to detect the pressure signals. The control system consists of a FGPA-based Speedgoat performance real-time target machine with an IO131 interface (16-bit inputs) controlled by the xPC target environment of MATLAB and SIMULINK and a homemade analog voltage to current convertor with a transconductance equal to 21.3 mA/V.

To identify the system's characteristic parameters (Bl, Z_{MS}, or Z_{MCL}), we first conduct three independent scattering measurements, for the loudspeaker to be controlled with three different electric loads plugged at its terminals. For the closed-box case, we use the standard two-microphone impedance measurement method. For the in-tube case, the impedance measurements require three simultaneous pressure measurements (p_{ref}, p^+, and p^-).

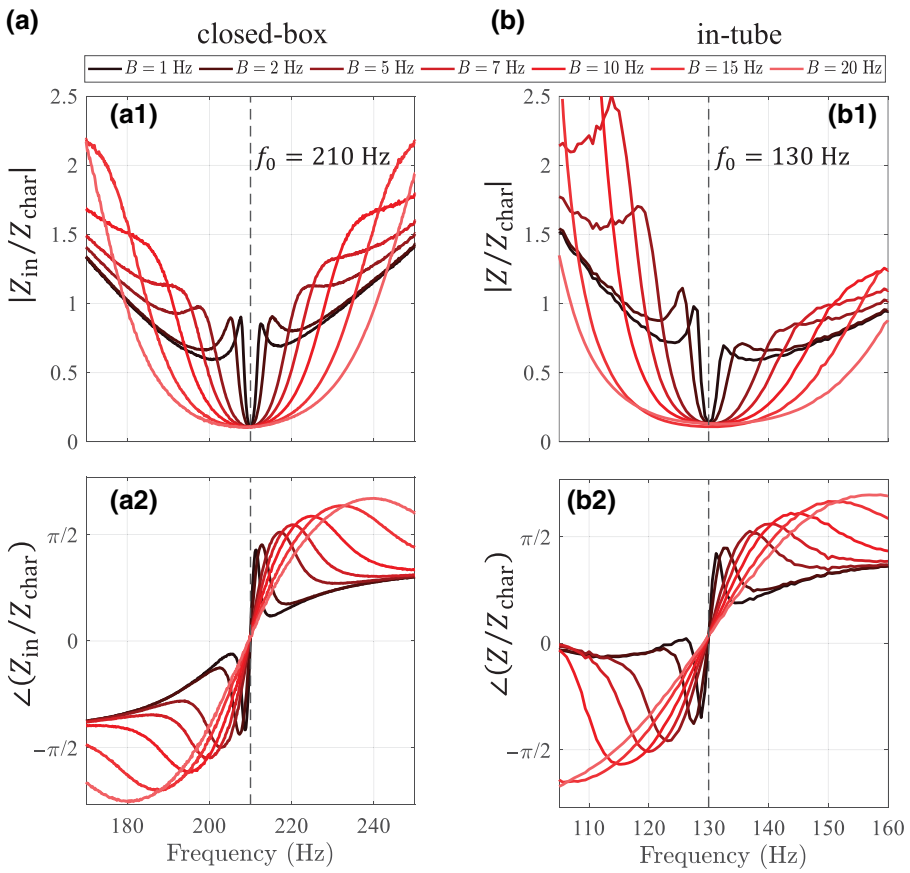

FIG. 6. Measured closed-box (a) and in-tube (b) electrodynamic loudspeaker impedance where the edge frequency of the Bessel filter B is shifted from 1 to 20 Hz. For the case of the closed-box system: $f_0 = 210$ Hz (represented by the dashed line) and $Z_{\text{in}}/Z_{\text{char}} = 0.1$. For the case of the in-tube system: $f_0 = 130$ Hz (represented by the dashed line) and $Z/Z_{\text{char}} = 0.15$. (a1), (b1) are graphical presentations of the amplitude and (a2), (b2) are of the phase of the acoustic impedance.

Hence, the formula for impedance can be easily derived directly from the transmission line (TL) model (Appendix) as $Z_{bc} = jZ_{\text{char}}\sin(kd)(p^+ - p^-)/[p_{\text{ref}} - \cos(kd)p^+]$, where d is the distance between p_{ref} and p^+ and k is the wave number (assuming p_{ref} is closer to the source than p^+). Based on the above sections and assuming polynomial fits for the unknown parameters, we derive a fit regarding the [120 Hz, 330 Hz] frequency range for the closed-box system and the [60 Hz, 230 Hz] frequency range for the in-tube system. The measured impedances and those calculated from the fitted parameters are seen in Fig. 4, thus demonstrating excellent agreement between measurements and our linear model.

We then start with a first set of experiments in which we demonstrate the possibility of controlling the resonance central frequency of such systems, i.e., control of the resonance frequency for a fixed bandwidth and real value of impedance at resonance. More precisely, in the case of the closed-box system, we fix the target impedance to $|Z_{\text{in}}/Z_{\text{char}}| = 0.1$, where Z_{in} is the input impedance of the loudspeaker and Z_{char} is the characteristic impedance, as defined in the Appendix. We target a low-loss resonator with a low residual acoustic resistance at resonance of 10% of the tube impedance. The edge frequency of the Bessel filter is set to $B = 10$ Hz, and we only ask the control to vary the value of the central frequency f_0. Notably, once these parameters are enforced on the system by the controller, the acoustic resonator is probed using microphones connected to a data acquisition system that is independent from the FPGA, and from the outside the system just looks like a normal passive mechanical acoustic resonator. In Fig. 5(a), we show the measured acoustic impedance for five independent experiments, each time with a central frequency of different value, namely, 200, 205, 210, 215, and 220 Hz. Evidently, the control mechanism provides the expected results, which can be seen clearly in Fig. 5(a2). The phase of the acoustic impedances crosses zero at the externally determined frequencies, while the measured impedance is at the targeted ratio and the bandwidth does not change. This corresponds to a system with almost unitary reflection, i.e., almost no absorption, at resonance. The measurements for the in-tube system are seen in Fig. 5(b). This time, we fix the target real impedance at $|Z/Z_{\text{char}}| = 0.15$, where Z is the impedance of the in-tube loudspeaker, and the edge frequency at $B = 5$ Hz. We exhibit five independent experiments similarly with the closed-box system, where the central frequency takes the values 120, 125, 130, 135, and 140 Hz. Again, the measurements agree with the expected results of the control mechanism in terms of the target real impedance value and constant bandwidth [Fig. 5(b1)] and the location of the resonance frequencies [Fig. 5(b2)]. In terms of

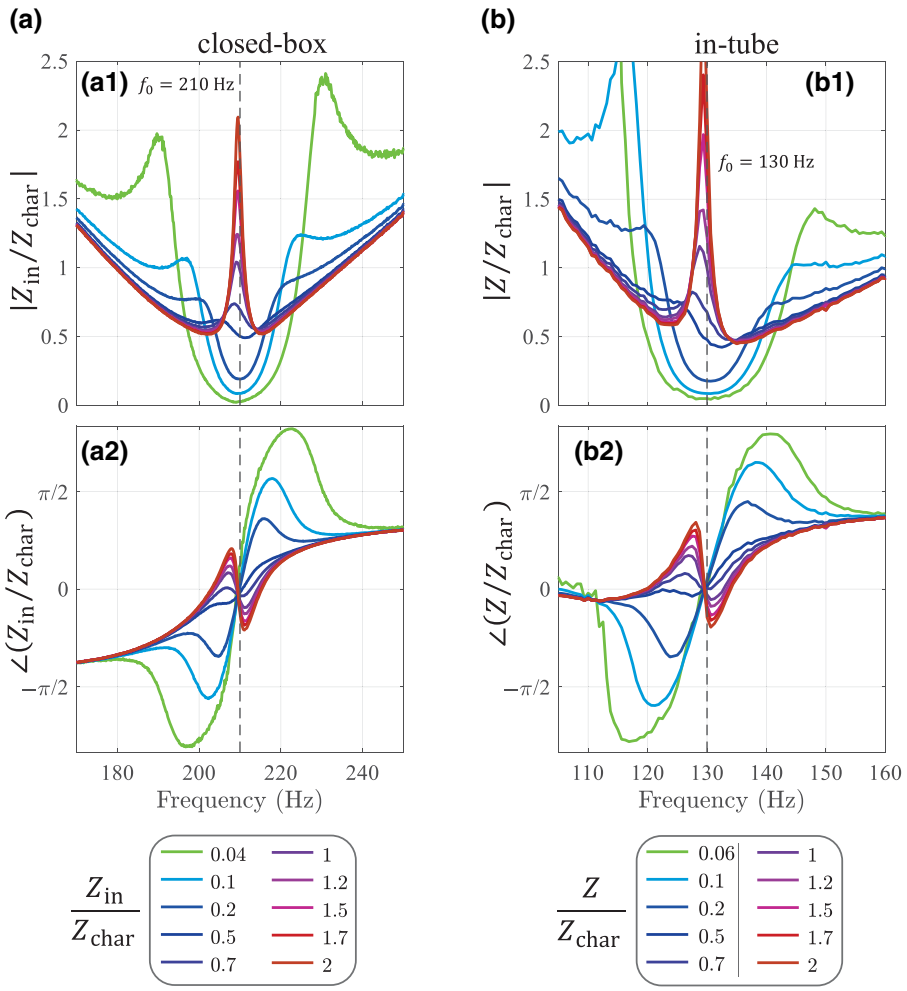

FIG. 7. Measured closed-box (a) and in-tube (b) electrodynamic loudspeaker impedance for control of the impedance at a specific frequency f_0. In the case of the closed-box system, the target impedance Z_{in}/Z_{char} is shifted from 0.04 to 2 at $f_0 = 210$ Hz with $B = 5$ Hz. In the case of the in-tube system, the target Z/Z_{char} is shifted from 0.06 to 2 at $f_0 = 130$ Hz with $B = 5$ Hz. (a1),(b1) are graphical presentations of the amplitude and (a2),(b2) are the phase of the acoustic impedance.

scattering, the total reflection, absorption, and transmission of this element depend also on the tube termination. For instance, in the case of an anechoic termination, this in-tube element would have a reflection coefficient of about 0.115 at resonance. Notably, also, since the loudspeaker is deeply subwavelength, its reflection is symmetric, despite its asymmetric geometry, and the control strategy works regardless of the wave direction.

Since f_0 is not the only reconfigurable element, we can also control the bandwidth of the resonators by tuning the edge of the Bessel filter (Fig. 6) at a fixed resonance frequency and real resonant target impedance. In Fig. 6(a), the measurements of the closed-box system are shown, while Fig. 6(b) reports those of the in-tube configuration. The measurements confirm that by changing the edge frequency of the filter we can easily control the bandwidth of the resonance. As expected, as the bandwidth opens up, the slope of the phase of the impedance decreases, although it always crosses zero at the same frequency.

Finally, in Fig. 7, we show the last possibility, namely, control of the targeted real impedance for a scenario of fixed central frequency and edge-filter frequency. The measurements show a wide range of achievable targets for the impedances, from values higher than the impedance of the tube all the way down to near zero. As the targeted impedances gradually increase, the slope of the phase of the impedances changes sign above a threshold value (above the physical acoustic impedance at the selected central frequency). Interestingly, the ability to target very low values corresponds to the possibility of creating resonators with almost no residual absorption at resonance, which is key in the development of applications of locally resonant metamaterials.

V. DISCUSSION

Here, we propose, analyze, and demonstrate a control mechanism to obtain active acoustic resonators with independently reconfigurable resonance frequency, absorption, and bandwidth. We illustrate experimentally the tunability of such systems by controlling the resonance frequency simply by changing the frequency, f_0, of a real-time modulation-demodulation scheme used in the feedback control loop. We also show that the bandwidth and real impedance at resonance can be reconfigured by changing the edge frequency, B, of the low-pass filter and the value

of the control coefficient Θ at f_0 (which can be calculated directly from the desired target resonance impedance ratio of $Z_{\text{in}}/Z_{\text{char}}$ for closed-box systems or Z/Z_{char} for in-tube systems). Since control is operated in the time domain, and only involves time-domain operations on sensed signals, it can be changed dynamically faster than the acoustic signal and used to create resonators with time-varying properties; this is also a current topic of interest in the physical community [26–30]. We therefore believe that the present work can largely enrich the toolbox of acoustic engineers and applied physicists, not only by building low-loss acoustic metamaterials out of active resonators with calibrated robust resonance frequencies and programmable bandwidth, but also by helping construct a new generation of dynamic acoustic systems, such as fast switches or time-modulated artificial structures with novel physical properties. At this point, we would also like to comment on some limitations of the approach. The first limit of the approach comes from our approximate knowledge of the system, which is modeled with a linear transfer function. Since this model can only approximate reality (especially due to the presence of nonlinearities), our control strategy has a certain margin of error. This becomes an issue when one wants to assign a value of impedance that is very different from that of the natural impedance of the uncontrolled loudspeaker because the feedback gain depends directly on their ratio. In practice, we note the need to refine our model when this ratio exceeds a factor of 10. The linear model is also expected to fail at high intensities, due to nonlinear phenomena that are not being accounted for. A more practical limitation of the method comes from the delay time of the FPGA, which sets a limit on the maximum operating frequency (around 10 kHz in our case). The 16-bit FPGA inputs also cause problems with very low intensities because they limit the signal-to-noise ratio. Finally, stability generally limits the maximum resonator bandwidth (bandwidth is a measure of the decay rate of the resonance, which is limited by what the scattering environment can provide). Notably, here, we have not targeted negative values of acoustic resistances (which would correspond to gain) because the experimental system, which only contains a single resonator, would become automatically unstable. However, in more complex systems with a less stringent stability condition, the method has been employed to induce acoustic gain [17]. We can thus envision that our strategy can be utilized to bridge the theoretical investigations of synthetic acoustic media and non-Hermitian sound-wave structures with pragmatic implementations.

ACKNOWLEDGMENTS

T.T.K. is grateful to Dr. B. Orazbayev for useful discussions. This work is supported by the Swiss National Science Foundation (SNSF) under Grant No. 172487.

APPENDIX: ACOUSTIC WAVE PROPAGATION MODEL

For completeness, we find it useful to recall here some important basic notions used throughout the paper. Sound waves that propagate in rigid cylindrical tubes with the wave function of the dominant mode are similar to plane waves (in contrast with the electromagnetic analog, in which transverse electric and magnetic (TEM) modes cannot be excited in closed waveguides). The requirements of excitation of the dominant mode are on the operating frequency. In other words, the frequency excitation at the source has to satisfy the condition $0 < f < 0.293c/a$, where a is the radius of the tube, $c = \sqrt{K_0/\rho_0}$ is the speed of sound, K_0 is the bulk modulus of the medium, and ρ_0 is the material density for isothermal flow [31–33]. Sound propagation in the frequency domain is governed by

$$\nabla p = -j\omega\rho_0\vec{u}, \tag{A1}$$

$$\nabla\vec{u} = -j\frac{\omega}{K_0}p, \tag{A2}$$

where p is the pressure disturbance, $\vec{u}$ is the particle velocity, and we assume a $e^{j\omega t}$ time convention. It is possible to model monomode sound propagation using a TL model, which is relevant in one-dimensional metamaterials that deal with subwavelength inclusions modeled as lumped-circuit elements. The TL model originates from electromagnetic and microwave circuit analysis and is used in a plethora of applications [34]. The model determines the voltage (V) and current (I) distributions of a line by taking into account the inductive (L) and capacitive (C) properties of the structure. The corresponding frequency-domain equations of a general transmission line model are

$$\frac{dV}{dz} = -jL\omega I, \tag{A3}$$

$$\frac{dI}{dz} = -jC\omega V. \tag{A4}$$

TABLE I. Analogies between electromagnetics (EM) and acoustics for the transmission line parameters.

EM model	Acoustic model
V (voltage)	p (pressure disturbance)
I (current)	Q (volume flux)
L (induction)	ρ_0/S_t (spring effect)
C (capacitance)	S_t/K_0 (mechanical compliance)
$\sqrt{L/C}$ (characteristic impedance, Z_{char})	$\sqrt{\rho_0 K_0}/S_t$ (characteristic impedance, Z_{char})
$1/\sqrt{LC}$ (speed of EM signal, c)	$\sqrt{K_0/\rho_0}$ (speed of sound, c)

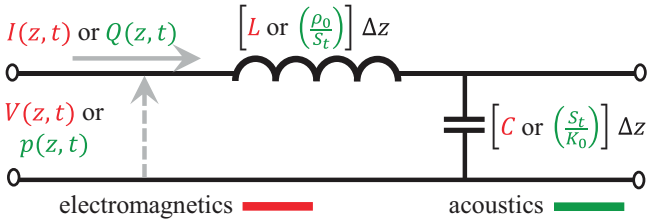

FIG. 8. Lumped element representation of electromagnetic (red) and acoustic (green) quantities for the TL model.

We can clearly note similarities between Eqs. (A1)–(A2) and Eqs. (A3)–(A4). The boundary conditions for the circuit and electromagnetic analysis of a TL ordain that V, I should be continuous when connecting two lines (due to Kirchhoff's laws and the electromagnetic boundary conditions). In distinction with circuits and electromagnetics, in acoustics, particle velocity can be discontinued. Nonetheless, the general continuity equation of flow commands instead that in the absence of sources the volume flux, $Q = \vec{u} \cdot \vec{S} = u_z S_t$ (where S_t is the cross-section area of the tube), is maintained [32]. This means that the acoustic quantity, which is continuous and directly linked to the current of the TL is the volume flux. One dimensional sound propagation inside rigid tubes, according to the TL mode, must therefore be expressed in terms of p and Q, and is thus given by

$$\frac{dp}{dz} = -j\,\omega \left(\frac{\rho_0}{S_t}\right) Q, \tag{A5}$$

$$\frac{dQ}{dz} = -j\,\omega \left(\frac{S_t}{K_0}\right) p. \tag{A6}$$

Taking into account Eqs. (A3)–(A6), it is accurate to identify the underlying equivalences between the TL parameters and those of acoustic propagation. We present in Table I the electromagnetic and acoustic analogies required for the TL model. In Fig. 8, we present schematically the TL parameters for the electromagnetic and the acoustic analog as lumped elements.

[1] S. A. Cummer, J. Christensen, and A. Alù, Controlling sound with acoustic metamaterials, Nat. Rev. Mater. **1**, 16001 (2016).

[2] P. A. Deymier, editor, *Acoustic Metamaterials and Phononic Crystals* (Springer, Berlin, Heidelberg, 2013).

[3] R. V. Craster and J. Kaplunov, editor, *Dynamic Localization Phenomena in Elasticity, Acoustics and Electromagnetism* (Springer, Vienna, 2013).

[4] G. Ma and P. Sheng, Acoustic metamaterials: From local resonances to broad horizons, Sci. Adv. **2**, e1501595 (2016).

[5] N. Jiménez, V. Romero-García, V. Pagneux, and J. P. Groby, Rainbow-trapping absorbers: Broadband, perfect and asymmetric sound absorption by subwavelength panels for transmission problems, Sci. Rep. **7**, 13595 (2017).

[6] V. Romero-García, C. Lagarrigue, J.-P. Groby, O. Richoux, and V. Tournat, Tunable acoustic waveguides in periodic arrays made of rigid square-rod scatterers: Theory and experimental realization, J. Phys. D. Appl. Phys. **46**, 305108 (2013).

[7] V. Romero-García, G. Theocharis, O. Richoux, A. Merkel, V. Tournat, and V. Pagneux, Perfect and broadband acoustic absorption by critically coupled sub-wavelength resonators, Sci. Rep. **6**, 19519 (2016).

[8] X. Hu, K.-M. Ho, C. T. Chan, and J. Zi, Homogenization of acoustic metamaterials of Helmholtz resonators in fluid, Phys. Rev. B **77**, 172301 (2008).

[9] F. Lemoult, N. Kaina, M. Fink, and G. Lerosey, Wave propagation control at the deep subwavelength scale in metamaterials, Nat. Phys. **9**, 55 (2013).

[10] J. Zhu, J. Christensen, J. Jung, L. Martin-Moreno, X. Yin, L. Fok, X. Zhang, and F. J. Garcia-Vidal, A holey-structured metamaterial for acoustic deep-subwavelength imaging, Nat. Phys. **7**, 52 (2011).

[11] F. Zangeneh-Nejad and R. Fleury, Active times for acoustic metamaterials, Rev. Phys. **4**, 100031 (2019).

[12] B. I. Popa, L. Zigoneanu, and S. A. Cummer, Tunable active acoustic metamaterials, Phys. Rev. B **88**, 024303 (2013).

[13] J. Christensen, M. Willatzen, V. R. Velasco, and M.-H. Lu, Parity-Time Synthetic Phononic Media, Phys. Rev. Lett. **116**, 207601 (2016).

[14] R. Fleury, D. L. Sounas, and A. Alù, An invisible acoustic sensor based on parity-time symmetry, Nat. Commun. **6**, 5905 (2015).

[15] M. Farhat, P. Y. Chen, S. Guenneau, S. Enoch, and A. Alù, Frequency-selective surface acoustic invisibility for three-dimensional immersed objects, Phys. Rev. B **86**, 174303 (2012).

[16] G. Ma, X. Fan, P. Sheng, and M. Fink, Shaping reverberating sound fields with an actively tunable metasurface, Proc. Natl Acad. Sci. U.S.A. **115**, 6638 (2018).

[17] E. Rivet, A. Brandstötter, K. G. Makris, H. Lissek, S. Rotter, and R. Fleury, Constant-pressure sound waves in non-Hermitian disordered media, Nat. Phys. **14**, 942 (2018).

[18] S. Yang, J. H. Page, Z. Liu, M. L. Cowan, C. T. Chan, and P. Sheng, Focusing of sound in a 3D phononic crystal, Phys. Rev. Lett. **93**, 024301 (2004).

[19] R. Thevamaran, R. M. Branscomb, E. Makri, P. Anzel, D. Christodoulides, T. Kottos, and E. L. Thomas, Asymmetric acoustic energy transport in non-Hermitian metamaterials, J. Acoust. Soc. Am. **146**, 863 (2019).

[20] F. Zangeneh-Nejad and R. Fleury, Performing mathematical operations using high-index acoustic metamaterials, New J. Phys. **20**, 073001 (2018).

[21] J. Li, C. Shen, A. Díaz-Rubio, S. A. Tretyakov, and S. A. Cummer, Systematic design and experimental demonstration of bianisotropic metasurfaces for scattering-free manipulation of acoustic wavefronts, Nat. Commun. **9**, 1342 (2018).

[22] N. Börsing, T. S. Becker, A. Curtis, D.-J. van Manen, T. Haag, and J. O. A. Robertsson, Cloaking and Holography Experiments Using Immersive Boundary Conditions, Phys. Rev. Appl. **12**, 024011 (2019).

[23] E. Rivet, S. Karkar, and H. Lissek, Broadband low-frequency electroacoustic absorbers through hybrid sensor-/shunt-based impedance control, IEEE Trans. Control Syst. Technol. **25**, 63 (2017).

[24] H. Lissek, R. Boulandet, and R. Fleury, Electroacoustic absorbers: Bridging the gap between shunt loudspeakers and active sound absorption, J. Acoust. Soc. Am. **129**, 2968 (2011).

[25] S. L. Hahn and K. M. Snopek, *Complex and Hypercomplex Analytic Signals: Theory and Applications* (Artech House, Boston, USA, 2017).

[26] R. Fleury, A. B. Khanikaev, and A. Alù, Floquet topological insulators for sound, Nat. Commun. **7**, 11744 (2016).

[27] T. T. Koutserimpas and R. Fleury, Zero refractive index in time-Floquet acoustic metamaterials, J. Appl. Phys. **123**, 091709 (2018).

[28] T. T. Koutserimpas, A. Alù, and R. Fleury, Parametric amplification and bidirectional invisibility in $\mathcal{PT}$-symmetric time-Floquet systems, Phys. Rev. A **97**, 013839 (2018).

[29] T. T. Koutserimpas and R. Fleury, Coupled-mode theory for stationary and nonstationary resonant sound propagation, Wave Motion **89**, 221 (2019).

[30] J. Li, C. Shen, X. Zhu, Y. Xie, and S. A. Cummer, Nonreciprocal sound propagation in space-time modulated media, Phys. Rev. B **99**, 144311 (2019).

[31] D. C. Gazis, Three-dimensional investigation of the propagation of waves in hollow circular cylinders. I. analytical foundation, J. Acoust. Soc. Am. **31**, 568 (1959).

[32] J. Billingham and A. C. King, *Wave Motion* (Cambridge University Press, Cambridge, United Kingdom, 2006).

[33] P. M. Morse and K. U. Ingard, *Theoretical Acoustics* (Princeton University Press, New Jersey, USA, 1986).

[34] D. M. Pozar, *Microwave Engineering* (Wiley, New Jersey, USA, 2012).